Characterization of A Murine Model of Endothelial Dysfunction Induced by Chronic Intraperitoneal Administration of Angiotensin II

Celeste Trejo-Moreno
Universidad Autónoma del Estado de Morelos
Enrique Jiménez-Ferrer
Mexican Social Security Institute
Gabriela Castro-Martínez
Universidad Autónoma del Estado de Morelos
Marisol Méndez-Martínez
Universidad Autónoma del Estado de Morelos
María Angélica Santana
Universidad Autónoma del Estado de Morelos
Gerardo Arrellín-Rosas
Panamerican University
José Pedraza-Chaverri
National Autonomous University of Mexico
Omar Medina-Campos
National Autonomous University of Mexico
Beatriz Hernández-Téllez
National Autonomous University of Mexico
Joel Barrita-Cruz
Universidad Autónoma del Estado de Morelos
Oscar Ramírez-Pliego
Universidad Autónoma del Estado de Morelos
Maribel Herrera-Ruíz
Mexican Social Security Institute
Gladis Fragoso
National Autonomous University of Mexico
Gabriela Rosas-Salgado (gabyrosas62@hotmail.com)
Universidad Autónoma del Estado de Morelos

Research Article

Keywords: Endothelial dysfunction, cardiovascular, SAHT

Posted Date: December 4th, 2020

DOI: https://doi.org/10.21203/rs.3.rs-115181/v1

Abstract

Endothelial dysfunction (ED) is a key factor for the development of cardiovascular diseases. Due to its chronic, life-threatening nature, ED only can be studied experimentally in animal models. Therefore, this work was aimed to characterize a murine model of ED induced by a daily intraperitoneal administration of angiotensin II (AGII) for 10 weeks. Oxidative stress, inflammation, vascular remodeling, hypertension, and damage to various target organs were evaluated in treated animals. The results indicated that a chronic intraperitoneal administration of AGII increases the production of ROS, ICAM-1 expression, the production of TNFα, IL1β, IL17A, IL4, TGFβ, and IL10, as well as blood pressure levels; it also promotes vascular remodeling and induces non-alcoholic fatty liver disease, glomerulosclerosis, and proliferative retinopathy. Therefore, the model herein proposed can be a representative model for ED; additionally, it is easy to implement, safe, rapid, and inexpensive.

Introduction

The endothelium is a single-cell lining that covers the internal surface of blood vessels, cardiac valves, and various body cavities [1]. It acts as a gatekeeper, sensing and responding to stimuli (physical or chemical, like changes in blood flow or pressure, inflammatory signals, or the levels of circulating hormones) and activating vasoactive systems that help maintaining vasomotor balance and homeostasis in vascular tissues. The endothelium produces both agonistic and antagonistic molecules that help keeping homeostasis [2,3]. When this balance is disrupted, it favors vasculature vasoconstriction, leukocyte adherence, platelet activation, mitogenesis, pro-oxidation, thrombosis, impaired coagulation, vascular inflammation, and atherosclerosis. This altered condition is known as endothelial dysfunction (ED), since it reduces the capacity of endothelium to maintain homeostasis and leads to the development of vascular diseases like systemic arterial hypertension (SAHT), renal dysfunction, and cerebrovascular diseases, which are the main causes of morbidity and mortality worldwide [1,4]. Angiotensin II (AGII), part of the renin-angiotensin-aldosterone system (RAAS) [5], is actively involved in the pathophysiology of cardiovascular and renal diseases [6]. It may be responsible for triggering ED and vascular inflammation by inducing oxidative stress, which in turn causes the upregulation of inflammatory mediators and cell growth factors [7]. The severity of this pathology and its consequences make necessary to find a suitable animal model to study the pathophysiology of ED and the action mechanisms of the drugs intended to control it [8].

The administration of exogenous AGII to induce hypertension or study its effects has been widely used, delivered to mice either through an osmotic pump [9] or by an AGII-coated pellet [10] implanted under the skin. The model herein presented is a cost-effective variant of this endocrine model of hypertension pharmacologically induced by a chronic administration of AGII [11] since instead of infusion via a pump or pellet, the hormone was administered by a daily intraperitoneal injection. This method is easy, safe, rapid, and inexpensive.

In this model, subject mice not only showed hypertension, but a complete ED condition, as evinced by prooxidant and proinflammatory activity, vascular remodeling, and damage to target organs.

Results

Chronic i.p. administration of AGII induces a prooxidant condition by increasing NOX2 and NOX4 transcription.

Oxidative stress plays an important role in the pathophysiology of ED and associated cardiovascular diseases (CVDs), like SAHT, atherosclerosis, diabetes, cardiac hypertrophy, heart failure, and ischemia-reperfusion [12]. NADPH oxidases seem to be especially important for redox signaling, and this protein family could be a specific therapeutic target [12]. Six homologous forms of NADPH oxidases constitute the NOX family, which shares the capacity to transport electrons across the plasma membrane to generate superoxide and other downstream ROS. From this family, NOX2 and NOX4 are expressed in the endothelium [13], and AGII has been reported to induce their transcription [14]. To analyze the expression of the NOX2 and NOX4 homologues in kidney, a real-time quantitative PCR assay was performed, with specific primers for NOX2 and NOX4 mRNAs. Primer specificity was confirmed by PCR amplification of the cloned cDNAs, where no cross-hybridization to other NOX cDNAs was observed (data not shown). The results of PCR analysis are shown in Figure 1. The expression of NOX2 (Fig. 1A) and NOX4 (Fig. 1B) mRNA showed a 4- and 5-fold increase, respectively, in the kidneys of AGII-treated mice with respect to control animals ($P < 0.05$).

AGII increased eNOS transcription levels.

Both eNOS and iNOS produce nitric oxide (NO), but under different conditions. The former is an endothelial constitutive enzyme, and in this case, NO helps maintaining tissue homeostasis. The latter enzyme produces NO as a response to the activation of pro-inflammatory cells after damage or inflammation [15]. AGII has been reported to influence the expression of all three NO synthase (NOS) isoforms in the long term [16]. To determine which NOS homologue was overexpressed in this model, the expression of both eNOS and iNOS mRNA in mouse kidney was quantified by RT-PCR. After AGII administration, eNOS expression (Supplementary Fig. S1A online) showed a 2.5-fold increase ($P < 0.05$) with respect to the control group. iNOS expression also increased, but not significantly (see Supplementary Fig. S1B online).

The main ROS source is xanthine oxidase.

Oxidative stress is a key trait of ED. To determine whether ROS were produced in this model, and which enzyme is responsible for its production, various enzymes reported as ROS producers were evaluated in kidney extracts by quantitative DHE oxidation. Protein extracts from control or AGII-treated mice were exposed to a set of substrates before measuring ROSmnb production (Fig. 2). ROS production increased almost 2 times in AGII-treated animals with respect to controls when the extracts were exposed to xanthine ($P < 0.01$). To confirm this result, the extract was incubated with xanthine and its competitive

inhibitor allopurinol, which reduced ROS production. No differences were observed when the extracts were incubated with NADH, arginine, nor succinate. These data suggest that xanthine oxidase is involved in ROS production in response to chronic AGII administration, as expected in an ED model.

Chronic i.p. AGII administration induces a proinflammatory condition.

Low-grade inflammation in the endothelium is a major contributor to the development of CVD [17]. It has been reported that CVD patients show increased plasma levels of cytokines like the tumor necrosis factor-alpha (TNFα) and interleukin 6 (IL6), as well as adhesion molecules like the intercellular adhesion molecule-1 (ICAM-1), the vascular cell adhesion molecule-1 (VCAM-1), and E-selectin, among other inflammatory markers [18]. Thus, inflammation, a central mechanism in the progression of ED and CVD [7], was also evaluated in this model. Pro-inflammatory status was assessed in mouse kidney samples obtained after the last BP measure. Cytokine concentrations were determined by ELISA in tissue homogenates; ICAM-1 was detected by immunohistochemistry, and ICAM-1 mRNA was quantified by RT-PCR. As shown in Figure 3, AGII-treated mice showed significantly increased TNFα (25.2%, Fig. 3A), IL1β (31.1%, Fig. 3B), IL17A (51.3%, Fig. 3E), IL4 (31.7%, Fig. 3F), TGFβ (27.4%, Fig. 3G), and IL10 (64.3%, Fig. 3H) levels with respect to untreated controls, while no differences were observed in IL6 (Fig. 3C) or IFNγ levels (Fig. 3D).

On the other hand, a 6-fold increase was observed in the expression of ICAM-1 mRNA in AGII-treated animals with respect to controls ($P < 0.05$, Fig. 4G). ICAM-1 was detected in perirenal fat tissue (Fig. 4D), renal capsule cells (Fig. 4E), and renal interstice cells (Fig. 4F), accompanied by an inflammatory cell infiltrate in renal capsule tissue (Fig. 4E), in the group treated with AGII, while in the control group (Fig. 4A-C) it was not detected. These results indicate that i.p. AGII administration induces an inflammatory condition, as expected in ED.

Chronic AGII administration leads to hypertension and vascular remodeling.

Hypertension induction is one of the most important parameters expected in this model, because it is the most common clinical parameter of ED. AGII is actively involved in the pathophysiology of SAHT, since it triggers increased ROS production by endothelial cells [19]. By reducing NO bioavailability, ROS production increases BP by a two-way mechanism: on one hand, they alter the inner and outer diameter of blood vessels, reducing their light (vascular remodeling) [20]; on the other hand, they affect the capacity of blood vessels to dilate in response to systemic conditions [15]. Acting together, both effects result in hypertension.

The measurements and calculations performed in histological slides of the BHA of the portal triad in mouse liver are shown in Figure 5 (panels A, E). Vascular remodeling was assessed by determining medial thickness, lumen percentage, and the media/lumen ratio (Fig. 5B-D, Fig. 5F-H). Medial thickness was calculated by subtracting the luminal BHA area from the total BHA area. As shown in Figure 5, neither the total BHA vascular area, medial thickness, nor lumen area (panels B, C, and F respectively) were affected by AGII administration, but a 2-fold decrease was observed in lumen percentage with

respect to control mice ($P < 0.05$, Fig. 5G). Medial thickness (Fig. 5D) and the media/lumen ratio (Fig 5H) showed a 1.3- and 3.7-fold increase, respectively, which indicate hypertrophic vascular remodeling [17]. These results suggest that chronic AGII administration induces vascular remodeling, a key part of ED, hindering the flow of blood through the vessels and thus promoting hypertension.

A time-course plot of BP values in control and AGII-treated mice is shown in Fig. 6. BP was measured at the beginning (week 0), the middle (week 5), and the end of experiment (week 10). A gradual increase of systolic BP (SBP, Fig. 6A) and diastolic BP (DBP, Fig. 6B) was observed in AGII-treated mice. On week 5, SBP and DBP increased by 15% (Fig. 6A) and 16% (Fig. 6B), respectively, with respect to control mice ($P < 0.05$). On week 10, SBP increased by 25% (Fig. 6A) and DBP increased by 24% (Fig. 6B, $P < 0.05$) with respect to control. These results indicate that this model is suitable to study SAHT and its causes, including vascular remodeling.

Chronic AGII administration provides an effective model of non-alcoholic fat liver disease, glomerulosclerosis, and proliferative retinopathy.

Historically, AGII has been regarded as a primary factor of tissue damage [21] in different organs: it increases ROS production; it also promotes upregulation in the expression of cytokines, cell adhesion molecules, and profibrotic factors like the transforming growth factor-β (TGFβ), which increases the synthesis of extracellular matrix proteins and promote macrophage activation and infiltration [22], among other harmful responses. The effects of AGII were assessed in kidneys, where AGII leads to chronic kidney disease (CKD) due to glomerulosclerosis [23, 24]; liver, where AGII promotes the development and progression of non-alcoholic fat liver disease (NAFLD) [25]; and the eye, where AGII induces proliferative retinopathy [26].

Glomerulosclerosis is a condition frequently resulting from ED; thus, AGII-induced kidney damage was assessed on Masson trichrome-stained perirenal fat tissue, capsules, perivascular connective tissue, and cortical glomeruli. The type of cells infiltrating the capsule was determined by PAS staining; finally, and a morphometric analysis of glomeruli was performed. As shown in Figure 7, AGII-treated mice exhibited signs of renal damage, including renal capsule thickening (Fig. 7F) due to edema, fiber deposition, and infiltration of mononuclear cells, mainly lymphocytes and macrophages, characteristic of CKDs like glomerulosclerosis [27]. Additionally, perivascular fibrosis (Fig. 7G), congestion of the tubulointerstitial zone (Fig. 7H) and points of mononuclear infiltration (macrophages and lymphocytes) among perirenal fat adipocytes (Fig. 7E) were observed, while in the control group these characteristics were not detected (Fig 7A-D).

AGII administration induced renal capsule thickening, which may be associated to the infiltration of inflammatory cells, mostly lymphocytes, macrophages, plasmatic cells, and fibroblasts, but also basophiles and neutrophils to a lesser extent (Supplementary Fig. S2B), while these cells were not observed in the control group (Fig. S2A). As shown in Supplementary Fig. S2 online, an increase in glomerular area (37.0%, Fig. S2D-E), glomerulus vascular region hypertrophy (52.1%, Fig. S2F), and

increased mesangial area (16.1%, Fig. S2G), all signs of glomerulosclerosis, were observed in AGII-treated mice compared to the control group (Fig. S2C, E-G).

On the other hand, three pathologic liver alterations were found in AGII-treated mice: 1) Steatosis with a perivascular pattern stemming from the central vein of the hepatic lobule (Fig. 8F); 2) thickening of trabeculae (Fig. 8H) and Glisson's capsule (Fig. 8I-J), and 3) lymphocytic microabscesses with central necrosis (Fig. 8G). All these alterations, steatohepatitis, inflammation, and fibrosis are pathological traits of non-alcoholic steatohepatitis (NASH), while these characteristics were not observed in the control group (Fig. 8A-E). The thickening of trabeculae and Glisson's capsule is due to fiber deposition and the infiltration of mononuclear cells like lymphocytes, macrophages, fibroblasts, and fibrocytes, which account for fibrosis (Fig. 8H-J), indicate the chronicity of the inflammatory event and the ongoing repairing process.

With respect to the eye, neovascularization is a hallmark of proliferative retinopathy, where the growth of abnormally formed blood vessels leads to hemorrhage, vision loss, and blindness [28, 29]. As shown in Supplementary Fig. S3, no significant differences in the number of blood vessels (Fig. S3A-B) were found between control and AGII-treated mice. However, AGII administration increased the formation of neovessels ($P < 0.05$, Fig. S3C-D).

Discussion

ED is characterized by alterations in endothelium activity that lead to reduced vasodilation, accompanied by oxidative stress and a proinflammatory, prothrombic status. ED is linked to CVDs like hypertension, coronary artery disease, chronic heart failure, peripheral artery disease, cerebral vascular disease, diabetes, and chronic renal failure [18, 30]. This makes necessary to have a well-characterized animal model that represents ED pathophysiological picture. The factor that triggers the pathophysiological process is the cornerstone of the experimental model. Thus, we proposed an overstimulation of RAAS as the triggering factor for permanent endothelial damage, and a chronic administration of sub-effective doses of AGII was the factor chosen to accomplish this. The mechanisms underlying the reduced vasodilator responses in ED include a reduced NO generation and oxidative stress [18]. Vasoactive peptides like AGII contribute to these damage mechanisms [18].

The main ROS sources in CVDs are NADPH oxidases, uncoupled NOS isoforms, xanthine oxidase, and mitochondria [30, 31]. NADPH oxidases are a family of enzyme complexes that catalyze the transfer of electrons from NADPH to molecular oxygen via their "NOX" catalytic subunit, generating $O_2^{\cdot -}$ and H_2O_2 [32]. Our data indicate that i.p. chronic administration of AGII increased the expression of NOX2 and NOX4 mRNA. An upregulation of these isoforms has been reported in response to AGII administration [32, 33]. Our results showed that AGII increased the expression of eNOS mRNA. This upregulation could be mediated by an activation of the mitogen-activated protein kinase 3/1 (MAPK3/1, also known as ERK1/2) induced by AGII [34, 35]. In turn, ERK1/2 activates eNOS transcription factors like the activator protein 1

(AP1) and SV40 virus promoter-specific transcription protein 1 (Sp1), which upregulate eNOS mRNA expression [34].

However, while AGII induced the overexpression of NOX2, NOX4, and eNOS mRNA, the main ROS source was xanthine oxidase. These responses could be related to a failure of the DHE method to detect the fluorescent emission signal. Although DHE can freely cross cell membranes, the ethidium cation generated after reduction by ROS is impermeant. Thus, the DHE method would not allow the detection of ROS generated by NOX2 and NOX4, since these enzymes generate ROS within intracellular compartments like phagosomes and the endoplasmic reticulum [36, 37]. AGII-induced activation of xanthine oxidase plays a key role in ED [38]. Initially, xanthine oxidase is synthesized as xanthine dehydrogenase (XDH), which is converted into xanthine oxidase (XO) by either reversible conformational changes or irreversible proteolysis [39]. AGII significantly increases the irreversible proteolytic conversion of XDH into XO and the ensuing ROS production [38, 40, 41].

On the other hand, chronic low-grade inflammation has a crucial role in the pathogenesis of ED and SAHT [42, 43]. AGII promotes oxidative stress, and the ROS produced activate several signaling pathways, including the mitogen-activated protein kinase (MAPK) family, tyrosine kinases, RhoA/Rho kinases, protein kinase B (AKT), which are key for activating the nuclear factor kappa B (NF-κB) [33, 44, 45]. NF-κB promotes the synthesis of IL1β, IL6, TNFα, C-reactive protein, E-selectin, ICAM-1, VCAM-1, and the monocyte chemoattractant protein-1 (MCP1), among other molecules. Thus, AGII is a proinflammatory stimulant that attracts immune cells to the vascular wall by enhancing the production of cytokines and adhesion molecules [18, 43]. The results in our model support this concept, since AGII-treated mice showed increased levels of inflammatory cytokines, ICAM-1 expression, and infiltration of immune cells (macrophages, lymphocytes, plasmatic cells, basophils and neutrophils) in the kidney, a well-known target organ for ED [46].

Moreover, the combined effect of AGII, oxidative stress, and inflammation induces fibrosis, as well as the proliferation and migration of vascular smooth muscle cells (VSMC), which further contribute to vascular remodeling [43, 47, 48]. AGII and ROS activate the ERK1/2, JNK and NF-kB signaling pathways, leading to the activation of matrix metalloproteinases (MMPs) and the production of growth factors like the epidermal growth factor (EGF), platelet-derived growth factor (PDGF), and insulin-like growth factor (IGF) [48, 49]. These molecules promote the accumulation of extracellular matrix proteins (collagen and fibronectin) and the proliferation and migration of VSMC, which result in vascular remodeling [17, 48, 50]. In this work, we demonstrated that a chronic administration of AGII induced vascular remodeling. Along with the vasoconstrictor effect of AGII itself, vascular remodeling induced alterations in the microvasculature, increasing peripheral vascular resistance and ultimately leading to SAHT.

AGII has intense effects on both the structure and function of microvasculature. The microvascular alterations caused by AGII have been linked to the end-organ damage seen in SAHT [51]. The effects of ED on kidney, liver, and eyes were replicated in our model. In the liver, AGII has been reported to favor the development and progression of NAFLD by increasing steatosis, inflammation, insulin resistance, and

fibrosis [25]. In the kidneys, AGII induces cell growth, inflammation, fibrosis, and vasoconstriction in post-glomerular arterioles (increasing glomerular hydraulic pressure and the ultrafiltration of plasma proteins) [52]; in addition, AGII leads to glomerulosclerosis by increasing mesangial volume [23, 24]. In the eye, AGII induced proliferative retinopathy, defined by the growth of new aberrant blood vessels susceptible to hemorrhage, leakage, and fibrosis, which limit retinal function [53]; in fact, hypertension is a major risk factor for retinopathy [53], and AGII has been linked to the pathogenesis of proliferative retinopathy [26, 54].

In summary, our results show that chronic administration of AGII by a daily intraperitoneal injection leads to endothelial dysfunction characterized by prooxidant and proinflammatory activity, vascular remodeling, hypertension and damage to targets organs.

Materials And Methods

Animals and housing.

All experiments were performed on 10-weeks-old, male C57BL/6J mice. The animals were housed in groups of five in standard polypropylene cages. The mice were maintained in a 12:12-h light-dark cycle, fed with standard rodent chow and allowed fresh water *ad libitum*. All procedures were performed in accordance to the guidelines established by the official Mexican regulation NOM-062-ZOO-1999 (technical specifications for production, care and use of laboratory animals). Experimental protocols were reviewed and approved by the Ethical Committee for the Care and Use of Laboratory Animals (Permit No. 005/2011) at the School of Medicine of Universidad Autónoma del estado de Morelos (FM-UAEM)

Control and experimental groups.

Each experiment was performed on 10-animal groups and lasted 10 weeks. The treatments were applied daily by the intraperitoneal (i.p.) route. Control mice only received isotonic saline solution (ISS), while the experimental group received 0.1 μg/kg of AGII.

Organ retrieving. After the last blood pressure (BP) measurement, the mice were perfused with cold PBS under surgical anesthesia (xylazine, 10 mg/kg, i.p.), and the liver and kidneys were obtained. For histopathological and immunohistochemical studies, the organs were fixed in Zamboni's solution (2.0% formaldehyde, 0.2% picric acid, pH 7.0). To measure oxidant stress and interleukin levels, the organs were weighed and frozen at −80° C until used. For real time PCR assays, the organs were preserved in Trizol reagent (Invitrogen, Carlsbad, CA, USA) and stored at −80 °C until RNA isolation.

Measuring the production of reactive oxygen species.

The kidneys were homogenized in ice-cold HEPES buffer (25 mM HEPES, 1 mM EDTA, and 0.1 mM phenyl-methyl-sulfonyl-fluoride). The homogenates were centrifuged at 6000 × *g* for 5 min at 4 °C, and the supernatant was obtained. The oxidation of dihydroethidium (DHE) to ethidium (Eth) was used to measure the production of reactive oxygen species (ROS) [55]. The supernatants (10 μl) were incubated

with DHE (0.2 mM), salmon teste DNA (10 mg/ml), and the substrate for xanthine oxidase (XO), mitochondrial respiratory enzymes, NADH oxidase, or nitric oxide synthase (NOS). Eth-DNA fluorescence was measured at an excitation wavelength of 480 nm and an emission wavelength of 610 nm at 37 °C for 30 min in a multimode microplate reader (Synergy HT, Biotek, Winooski, VT, USA). Xanthine (0.1 mM) was used as a substrate for XO, and allopurinol (1 mM) was used as an XO inhibitor. Succinate (5 mM) was used as a substrate for mitochondrial ROS production. L-arginine (L-arg, 1 mM) was used as a substrate for NOS, and NADH (0.1 mM) was used as a substrate for NADH oxidase. A blank with no sample was used to measure background fluorescence, and this value was subtracted from each sample reading. Enzyme activity is expressed relative to the control.

Real time RT-PCR.

Total RNA was obtained from kidneys using Trizol, following the manufacturer's instructions. cDNA was synthesized from 2 μg of total RNA under standard reverse transcription conditions, using oligo(dT) in a final volume of 25 μl. cDNA was diluted 1:3, and 2 μl of the diluted sample were used for amplification, using the SYBR Green PCR Master Mix (Life Technologies, Carlsbad, CA, USA) and the following primers: *NOX2*, forward 5'-AGG AGT GCC CAG TAC CAA AGT-3', reverse 5'-TAC TGT CCC ACC TCC ATC TTG-3'; *NOX4*, forward 5'-ACC CAA GTT CCA AGC TCA TTT-3', reverse 5'-ATG GTG ACA GGT TTG TTG CTC-3'; *iNOS*, forward 5'-CCA AGC CCT CAC CTA CTT CC-3', reverse 5'-CTC TGA GGG CTG ACA CAA GG-3'; *eNOS*, forward 5'-CAA CGC TAC CAC GAG GAC ATT-3', reverse 5'-CTC CTG CAA AGA AAA GCT CTG G-3'; *ICAM-1*, forward 5'-GTG ATG CTC AGG TAT CCA TCC A-3', reverse 5'-CAC AGT TCT CAA AGC ACA GCG-3' (Sigma-Aldrich, St. Louis, MO, USA). The expression of the housekeeping gene glyceraldehyde-3-phosphate dehydrogenase (*GAPD*) was also evaluated as an internal control (4352932, Applied Biosystems, Foster City, CA, USA). mRNA levels were calculated from standard curves for each gene, relative to those of GAPD.

Blood pressure measurement.

Systolic and diastolic BP was measured daily within the 11:00-15:00-hours interval, to minimize circadian cycle-related variability [56], under surgical anesthesia (xylazine, 10 mg/kg, i.p.); the animals were kept on a heat pad at 33-34 °C and under a cotton towel to prevent heat loss. Systolic and diastolic BP values were recorded by the tail-cuff technique in a LE5002 system (Panlab, Barcelona, Spain) at the beginning (baseline) and every 5 weeks (on week 0, 5, and 10) until the end of the experiment. Two weeks before the baseline BP measurement and the first AGII application, the mice were subjected to two training sessions, one week apart. Mice with a BP increase of 15% or higher with respect to the baseline (time 0) were considered as hypertensive.

Histopathology.

After the last BP measurement, the mice were anesthetized with sodium pentobarbital (30 mg/kg, i.p.) and perfused with ice-cold PBS (NaCl 140 mM, KCl 2 mM, K_2HPO_4 1.15 mM). The kidneys and livers were removed and fixed in Zamboni's solution. Then, the tissues were dehydrated and embedded in paraffin.

Tissue sections (5 μm) were transferred to poly-L-lysine-coated slides (Sigma) and were deparaffinized and rehydrated. For histopathological studies, the slides were stained with either the Masson trichrome (kidney and liver), hematoxylin-eosin (eyes), or periodic acid-Schiff (PAS) stain (kidney). The Masson trichrome method combines hematoxylin stain with a cytoplasmic stain and a selective stain for connective tissue [57]. The PAS stain, which detects polysaccharides (glycogen and mucosal substances like glycoproteins, glycolipids, and mucins) in tissues to identify alterations in the basement membrane [58], was used to assess the expansion of the mesangial matrix by the presence of increased amounts of PAS-positive material in the mesangial region [59]. All slides were observed under an ECLIPSE 80i microscope (Nikon, Tokyo, Japan) and analyzed with the software Metamorph v.6.1. (Molecular Devices, San Jose, CA, USA).

Glomerulosclerosis or hyalinization was defined as the disappearance of cellular elements from the tuft, a collapse of capillary lumen, and a folding of the glomerular basement membrane with entrapment of amorphous material, as proposed by Raij et al. [59]. Glomerular injury was also analyzed according to the method proposed by that author, with minor modifications. Briefly, 50-60 cortical glomeruli were evaluated in PAS-stained kidney slides from each group under a 100X objective. Digitized images were analyzed with Metamorph v.6.1. The mesangial area was calculated by subtracting the capillary area from the total area. The results were expressed as percentage with respect to the total area.

Vascular remodeling was evaluated in the portal triad in Masson-stained liver slides. Total and luminal areas of the branch of hepatic artery (BHA) were measured in 10 slides per group under the 40X objective. The area corresponding to vessel thickness was determined by subtracting these two values. Lumen percentage, medial thickness percentage, and media/lumen ratio were calculated to assess vascular remodeling [60].

ICAM-1 detection by immunohistochemistry.

After deparaffinization and rehydration, tissue sections were incubated with 3% H_2O_2 and with 5% albumin with 1% Tween 20-PBS. After treatment, tissue sections were incubated overnight with rat anti-mouse ICAM-1 monoclonal antibody (eBioscence; CAT #: 16-0542) diluted 1:100 in 0.1% albumin, 0.05% Tween 20-PBS. After washing with PBS, the tissues were incubated with a biotinylated goat anti-rat IgG secondary antibody (MP Biomedicals, Santa Ana, CA, USA) diluted 1:1000, followed by HRP-labeled streptavidin solution (MP Biomedicals) at 37 °C for 30 min, and developed with 3,3-DAB (Zymed, San Francisco, CA, USA). All slides were counterstained with hematoxylin-eosin and photographed using an ECLIPSE 80i microscope and analyzed with Metamorph v.6.1.

Cytokine quantification by ELISA.

Kidneys were weighed and frozen at −80 °C until used. The organs were macerated in a frozen mortar with ice-cold PBS-PMSF (0.1%) 1:5 w/v. The suspensions were centrifuged, and supernatants were recovered and frozen at −20 °C until used. Various ELISA kits were used to determine cytokine concentration, following the manufacturer's instructions. OptEIA Mouse IL1β, IL4, IL6, IL10, IFNγ, and

TNFα ELISA kits were purchased from BD (Franklin Lakes, NJ, USA), while mouse IL17A and TGFβ ELISA kits were purchased from Applied Biosystems (Foster City, CA, USA). Briefly, 96-well flat-bottomed ELISA plates were coated with the respective capture antibody and incubated overnight at 4 °C. Non-specific binding sites were blocked by incubating for 30 minutes at RT with PBS-5% fetal bovine serum. Aqueous kidney extracts were added and incubated for 2 h at RT. Then, the plates were incubated with the corresponding detection anti-cytokine-HRP antibodies for 30 min at RT. Bound complexes were detected by reaction with tetramethylbenzidine substrate after 30 min of incubation in the darkness. The reaction was stopped with H_2SO_4 2N and absorbance was measured at 450 nm at 37 °C in a VERSAmax ELISA plate reader (Molecular Devices). Cytokine concentration was calculated according to standard curves for each cytokine and reported as pg/mg protein.

Statistical analysis.

Data were analyzed using the software InStat (GraphPad, San Diego, CA, USA). Data are reported as mean ± standard deviation (SD). An unpaired, two-tailed Student's *t*-test was used to compare groups. $P < 0.05$ was considered as statistically significant.

Declarations

Acknowledgments

The authors thank Biol. Nancy Arias García for her help in animal care; H.T. Noemí Gelista Herrera, M.Sc. Vanesa Báez Gelista, and Dr. Juan Carlos Báez Reyes for their help in slide preparation and histological procedures, and Juan Francisco Rodriguez for copyediting this manuscript.

Author contributions

Conceived and designed the experiments: EJF GRS. Performed the experiments: CTM GCM MMM ONMC BHT ORP. Analyzed the data: CTM GCM MMM MAS GAR JPC JBC EJF MHR GF GRS. Contributed reagents/materials/analysis tools: MAS JPC MHR. Writing – original draft: CTM, GF, GRS. Writing – review & editing: EJF, MHR, GF, GRS.

Competing interests.

The authors have declared that no competing interests exist.

Additional information

Correspondence and requests for materials should be addressed to G.R.S

References

1. Esper, R. J., *et al*. Endothelial dysfunction: a comprehensive appraisal. *Diabetol.***5**, 4. https://doi.org/10.1186/1475-2840-5-4 (2006).
2. Gibbons, G. H. Endothelial function as a determinant of vascular function and structure: a new therapeutic target. *J. Cardiol.***79**, 3–8. https://doi.org/10.1016/s0002-9149(97)00122-7 (1997).
3. Rubanyi, G. M. The role of endothelium in cardiovascular homeostasis and diseases. *Cardiovasc. Pharmacol.***22**, S1–S14. https://doi.org/10.1097/00005344-199322004-00002 (1993).
4. Verma, S., & Anderson, T. J. Fundamentals of endothelial function for the clinical cardiologist. *Circulation*. ***105***, 546–549. https://doi.org/10.1161/hc0502.104540 (2002).
5. Cody, R. J. The integrated effects of angiotensin II. *J. Cardiol.* ***79*****,** 9–11. https://doi.org/10.1016/s0002-9149(97)00123-9 (1997).
6. Kim, S., & Iwao, H. Molecular and cellular mechanisms of angiotensin II-mediated cardiovascular and renal diseases. *Rev.* **52**, 11–34. (2000).
7. Savoia, C., *et al*. Vascular inflammation and endothelial dysfunction in experimental hypertension. *J. Hypertens.***2011**, 281240. https://doi.org/10.4061/2011/281240 (2011).
8. Dornas, W. C., & Silva, M. E. Animal models for the study of arterial hypertension. *Biosci*. **36**, 731–737. https://doi.org/10.1007/s12038-011-9097-y (2011).
9. Landmesser, U., *et al*. Role of p47(phox) in vascular oxidative stress and hypertension caused by angiotensin II. *Hypertension*. **40**, 511–515. https://doi.org/10.1161/01.hyp.0000032100.23772.98 (2002).
10. Ichihara, S., *et al*. Angiotensin II type 2 receptor is essential for left ventricular hypertrophy and cardiac fibrosis in chronic angiotensin II-induced hypertension. *Circulation*, **104**, 346–351. https://doi.org/10.1161/01.cir.104.3.346 (2001).
11. McCubbin, J. W., DeMoura, R. S., Page, I. H., & Olmsted, F. Arterial hypertension elicited by subpressor amounts of angiotensin. **149**, 1394–1395. https://doi.org/10.1126/science.149.3690.1394 (1965).
12. Cave, A. C., *et al*. NADPH oxidases in cardiovascular health and disease. *Redox. Signal.***8**, 691–728. https://doi.org/10.1089/ars.2006.8.691 (2006).
13. Bedard, K., & Krause, K. H. The NOX family of ROS-generating NADPH oxidases: physiology and pathophysiology. *Physiol Rev.***87**, 245–313. https://doi.org/10.1152/physrev.00044.2005 (2007).
14. Nguyen Dinh Cat, A., Montezano, A. C., Burger, D., & Touyz, R. M. Angiotensin II, NADPH oxidase, and redox signaling in the vasculature. *Redox. Signal.***19**, 1110–1120. https://doi.org/10.1089/ars.2012.4641 (2013).
15. Lind, M., *et al*. Inducible nitric oxide synthase: Good or bad?. *Biomed Pharmacother.***93**, 370–375. https://doi.org/10.1016/j.biopha.2017.06.036 (2017).
16. Millatt, L. J., Abdel-Rahman, E. M., & Siragy, H. M. Angiotensin II and nitric oxide: a question of balance. *Pept.***81**, 1–10. https://doi.org/10.1016/s0167-0115(99)00027-0 (1999).
17. Zhang, C. The role of inflammatory cytokines in endothelial dysfunction. *Basic Res. Cardiol.* **103**, 398–406. https://doi.org/10.1007/s00395-008-0733-0 (2008).

18. Endemann, D. H., & Schiffrin, E. L. Endothelial dysfunction. *Am. Soc. Nephrol.* **15**, 1983–1992. https://doi.org/10.1097/01.ASN.0000132474.50966.DA (2004).
19. Masi, S., Uliana, M., & Virdis, A. Angiotensin II and vascular damage in hypertension: Role of oxidative stress and sympathetic activation. *Pharmacol.***115**, 13–17. https://doi.org/10.1016/j.vph.2019.01.004 (2019).
20. Didion S. P. New Insights Into Mechanisms Associated With Angiotensin II-Induced Vascular Hypertrophy and Remodeling. **67**, 501–503. https://doi.org/10.1161/HYPERTENSIONAHA.115.06737 (2016).
21. Struthers, A. D., & MacDonald, T. M. Review of aldosterone- and angiotensin II-induced target organ damage and prevention. *Res.* **61**, 663–670. https://doi.org/10.1016/j.cardiores.2003.11.037 (2004).
22. Ruiz-Ortega, M., Lorenzo, O., Suzuki, Y., Rupérez, M., & Egido, J. Proinflammatory actions of angiotensins. *Opin. Nepphrol. Hypertens.* **10**, 321–329. https://doi.org/10.1097/00041552-200105000-00005 (2001).
23. Anderson, P. W., Do, Y. S., & Hsueh, W. A. Angiotensin II causes mesangial cell hypertrophy. **21**, 29–35. https://doi.org/10.1161/01.hyp.21.1.29 (1993).
24. Orth, S. R., Weinreich, T., Bönisch, S., Weih, M., & Ritz, E. Angiotensin II induces hypertrophy and hyperplasia in adult human mesangial cells. *Exp Nephrol.***3**, 23–33. (1995).
25. Matthew Morris, E., Fletcher, J. A., Thyfault, J. P., & Rector, R. S. The role of angiotensin II in nonalcoholic steatohepatitis. *Cell. Endocrinol.***378**, 29–40. https://doi.org/10.1016/j.mce.2012.04.013 (2013).
26. Fernandez, L. A., Twickler, J., & Mead, A. Neovascularization produced by angiotensin II. *Lab. Clin. Med.* **105**, 141–145. (1985).
27. Karanovic, D., et al. Effects of Single and Combined Losartan and Tempol Treatments on Oxidative Stress, Kidney Structure and Function in Spontaneously Hypertensive Rats with Early Course of Proteinuric Nephropathy. *PloS one*. **11**, e0161706. https://doi.org/10.1371/journal.pone.0161706 (2016).
28. Amaral, S. L., Papanek, P. E., & Greene, A. S. Angiotensin II and VEGF are involved in angiogenesis induced by short-term exercise training. *J. Ohysiol. Heart Circ. Physiol.***281**, H1163–H1169. https://doi.org/10.1152/ajpheart.2001.281.3.H1163 (2001).
29. Deliyanti, D., *et al*. Neovascularization is attenuated with aldosterone synthase inhibition in rats with retinopathy. *Hypertension* **59**, 607–613. https://doi.org/10.1161/HYPERTENSIONAHA.111.188136 (2012).
30. Zalba, G., et al. Oxidative stress, endothelial dysfunction and cerebrovascular disease. *Dis.***24**, 24–29. https://doi.org/10.1159/000107376 (2007).
31. Burtenshaw, D., Hakimjavadi, R., Redmond, E. M., & Cahill, P. A. Nox, Reactive Oxygen Species and Regulation of Vascular Cell Fate. **6**, 90. https://doi.org/10.3390/antiox6040090 (2017).
32. Dikalov, S. I., et al. Nox2-induced production of mitochondrial superoxide in angiotensin II-mediated endothelial oxidative stress and hypertension. *Redox. Signal.* **20**, 281–294.

https://doi.org/10.1089/ars.2012.4918 (2014).

33. Montezano, A. C., & Touyz, R. M. Reactive oxygen species, vascular Noxs, and hypertension: focus on translational and clinical research. *Redox. Signal.***20**, 164–182. https://doi.org/10.1089/ars.2013.5302 (2014).
34. Yang, S. H., Sharrocks, A. D., & Whitmarsh, A. J. Transcriptional regulation by the MAP kinase signaling cascades. **320**, 3–21. https://doi.org/10.1016/s0378-1119(03)00816-3 (2003).
35. Zheng, J., Wen, Y., Chen, D. B., Bird, I. M., & Magness, R. R. Angiotensin II elevates nitric oxide synthase 3 expression and nitric oxide production via a mitogen-activated protein kinase cascade in ovine fetoplacental artery endothelial cells. *Reprod.***72**, 1421–1428. https://doi.org/10.1095/biolreprod.104.039172 (2005).
36. Serrander, L., et al. NOX4 activity is determined by mRNA levels and reveals a unique pattern of ROS generation. *J.***406**, 105–114. https://doi.org/10.1042/BJ20061903 (2007).
37. Rinaldi, M., Moroni, P., Paape, M. J., & Bannerman, D. D. Evaluation of assays for the measurement of bovine neutrophil reactive oxygen species. *Immunol. Immunopathol.***115**, 107–125. https://doi.org/10.1016/j.vetimm.2006.09.009 (2007).
38. Landmesser, U., et al. Angiotensin II induces endothelial xanthine oxidase activation: role for endothelial dysfunction in patients with coronary disease. *Thromb. Vasc. Biol.***27**, 943–948. https://doi.org/10.1161/01.ATV.0000258415.32883.bf (2007).
39. Dikalov, S.I., Harrison, D.G. *Systems Biology of Free Radicals and Antioxidants*. (ed. Laher, I.) 1255-1271 (Springer, 2014).
40. McNally, J. S., Saxena, A., Cai, H., Dikalov, S., & Harrison, D. G. Regulation of xanthine oxidoreductase protein expression by hydrogen peroxide and calcium. *Thromb. Vasc. Biol.***25**, 1623–1628. https://doi.org/10.1161/01.ATV.0000170827.16296.6e (2005).
41. Kondo, M., et al. Xanthine Oxidase Inhibition by Febuxostat in Macrophages Suppresses Angiotensin II-Induced Aortic Fibrosis. *J. Hypertens.* **32**, 249–256. https://doi.org/10.1093/ajh/hpy157 (2019).
42. Hernanz, R., et al. Toll-like receptor 4 contributes to vascular remodelling and endothelial dysfunction in angiotensin II-induced hypertension. *J. Pharmacol.* **172**, 3159–3176. https://doi.org/10.1111/bph.13117 (2015).
43. Kröller-Schön, S., et al. Endothelial α1AMPK modulates angiotensin II-mediated vascular inflammation and dysfunction. *Basic Res. Cardiol.* **114**, 8. https://doi.org/10.1007/s00395-019-0717-2 (2019).
44. Ushio-Fukai, M., et al. Reactive oxygen species mediate the activation of Akt/protein kinase B by angiotensin II in vascular smooth muscle cells. *Biol. Chem.***274**, 22699–22704. https://doi.org/10.1074/jbc.274.32.22699 (1999).
45. Trejo-Moreno, C., et al. Cucumis sativus Aqueous Fraction Inhibits Angiotensin II-Induced Inflammation and Oxidative Stress In Vitro. **10**, 276. https://doi.org/10.3390/nu10030276 (2018).
46. Henke, N., et al. Vascular endothelial cell-specific NF-kappaB suppression attenuates hypertension-induced renal damage. *Res.* **101**, 268–276. https://doi.org/10.1161/CIRCRESAHA.107.150474

(2007).

47. Williams B. Angiotensin II and the pathophysiology of cardiovascular remodeling. *J. Cardiol.***87**, 10C–17C. https://doi.org/10.1016/s0002-9149(01)01507-7 (2001).
48. Dong, H., Ming, S., Fang, J., Li, Y., & Liu, L. Icariin ameliorates angiotensin II-induced cerebrovascular remodeling by inhibiting Nox2-containing NADPH oxidase activation. *Cell.***32**, 22–30. https://doi.org/10.1007/s13577-018-0220-3 (2019).
49. Touyz, R. M. Reactive oxygen species as mediators of calcium signaling by angiotensin II: implications in vascular physiology and pathophysiology. *Redox. Signal.***7**, 1302–1314. https://doi.org/10.1089/ars.2005.7.1302 (2005).
50. Pires, P. W., Deutsch, C., McClain, J. L., Rogers, C. T., & Dorrance, A. M. Tempol, a superoxide dismutase mimetic, prevents cerebral vessel remodeling in hypertensive rats. *Res.***80**, 445–452. https://doi.org/10.1016/j.mvr.2010.06.004 (2010).
51. Cheung, C. Y., Ikram, M. K., Sabanayagam, C., & Wong, T. Y. Retinal microvasculature as a model to study the manifestations of hypertension. **60**, 1094–1103. https://doi.org/10.1161/HYPERTENSIONAHA.111.189142 (2012).
52. Remuzzi, G., Perico, N., Macia, M., & Ruggenenti, P. The role of renin-angiotensin-aldosterone system in the progression of chronic kidney disease. *Kidney Int. Suppl.***68**, S57–S65. https://doi.org/10.1111/j.1523-1755.2005.09911.x (2005).
53. Lovshin, J. A., et al. Retinopathy and RAAS Activation: Results From the Canadian Study of Longevity in Type 1 Diabetes. *Diabetes Care*. **42**, 273–280. https://doi.org/10.2337/dc18-1809 (2019).
54. Nagai, N., et al. Selective suppression of pathologic, but not physiologic, retinal neovascularization by blocking the angiotensin II type 1 receptor. *Ophthalmol. Vis. Sci.***46**, 1078–1084. https://doi.org/10.1167/iovs.04-1101 (2005).
55. Satoh, M., *et al*. NAD(P)H oxidase and uncoupled nitric oxide synthase are major sources of glomerular superoxide in rats with experimental diabetic nephropathy. *J. Physiol. Renal Physiol.***288**, F1144–F1152. https://doi.org/10.1152/ajprenal.00221.2004 (2005).
56. Marques, F. Z., *et al*. Genes influencing circadian differences in blood pressure in hypertensive mice. *PloS one*, **6**, e19203. https://doi.org/10.1371/journal.pone.0019203 (2011).
57. Goldner J. A modification of the masson trichrome technique for routine laboratory purposes. *J. Pathol.***14**, 237–243. (1938).
58. Feldman, D. L., & Christian, J. J. The development of an acth-induced renal glomerular lesion in Mus musculus. An ultrastructural study. *Pathol***134**, 181–197. https://doi.org/10.1002/path.1711340303 . (1981).
59. Raij, L., Azar, S., & Keane, W. Mesangial immune injury, hypertension, and progressive glomerular damage in Dahl rats. *Kidney Int*. **26**, 137–143. https://doi.org/10.1038/ki.1984.147 (1984).
60. Intengan, H. D., & Schiffrin, E. L. Vascular remodeling in hypertension: roles of apoptosis, inflammation, and fibrosis. **38**, 581–587. https://doi.org/10.1161/hy09t1.096249 (2001).

Figures

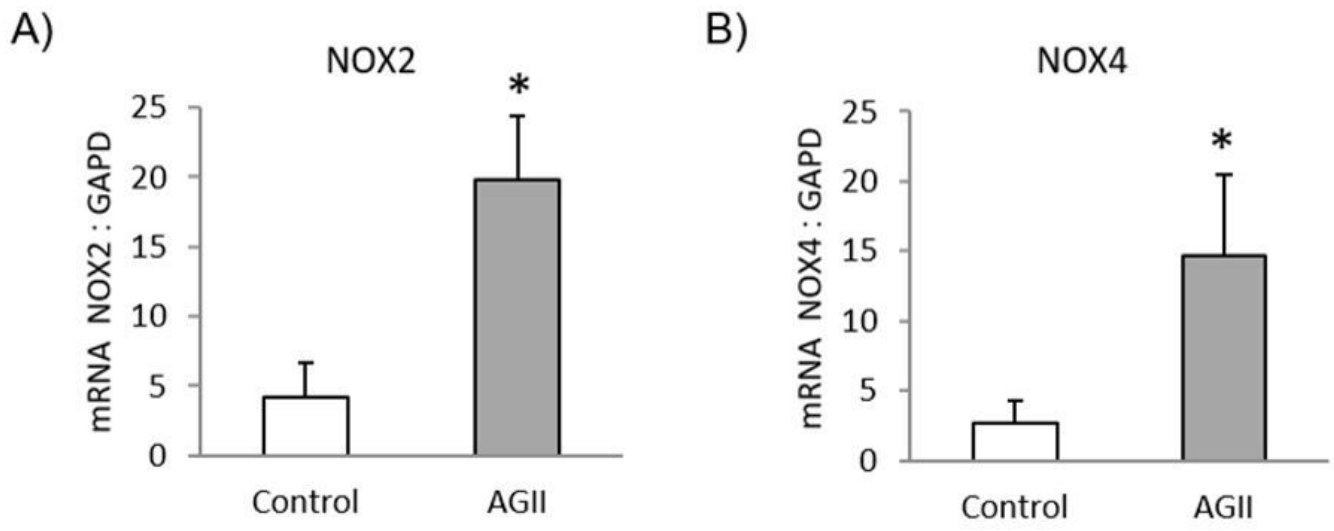

Figure 1

Chronic AGII administration increases the expression of NOX2 and NOX4 mRNA in kidney. Data are reported as mean ± SD and analyzed with a two-tailed, unpaired Student's t test ($P < 0.05$). * indicate differences with respect to control.

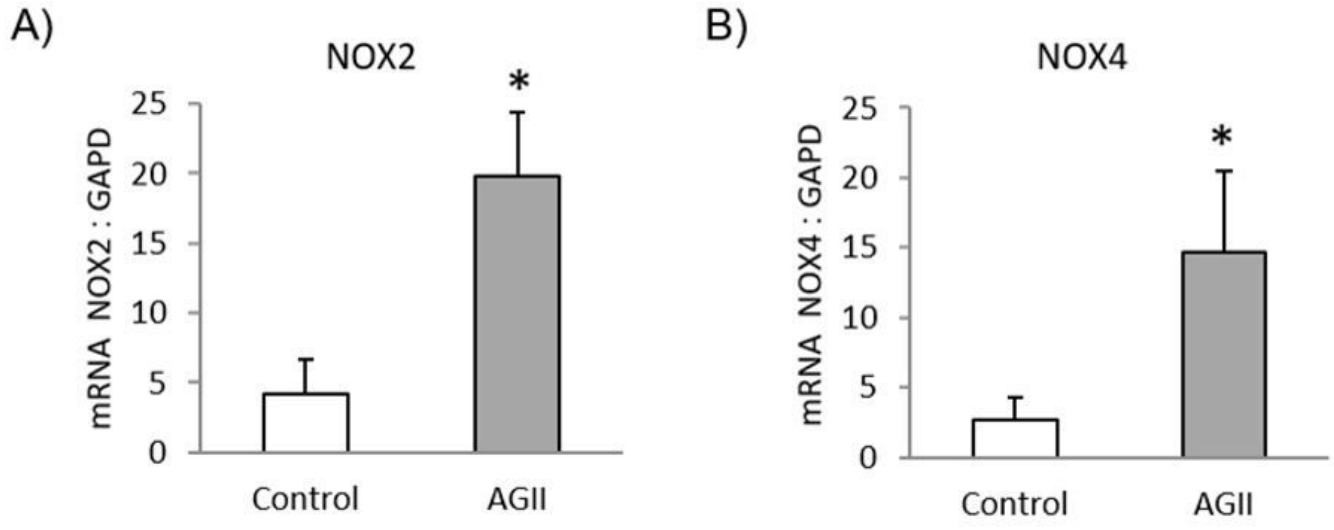

Figure 1

Chronic AGII administration increases the expression of NOX2 and NOX4 mRNA in kidney. Data are reported as mean ± SD and analyzed with a two-tailed, unpaired Student's t test ($P < 0.05$). * indicate

differences with respect to control.

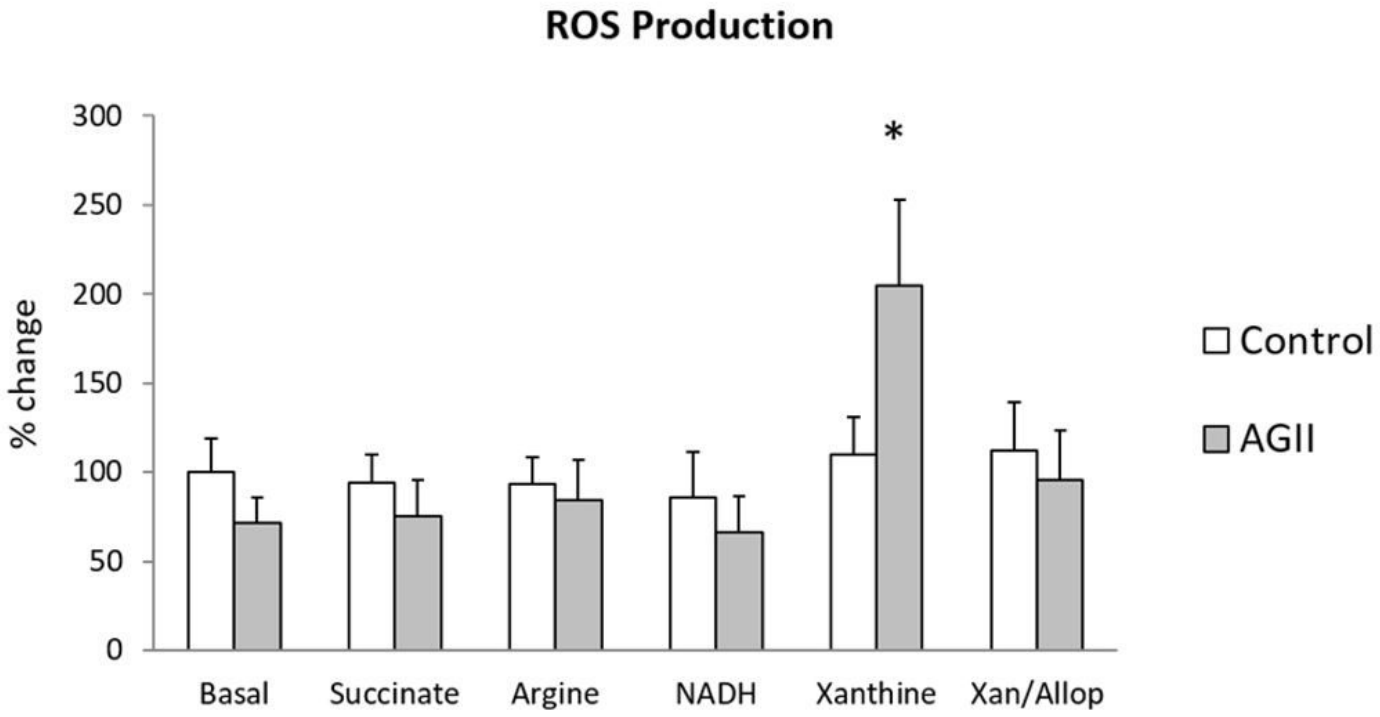

Figure 2

ROS production. AGII failed to induce changes in ROS production when NADH, arginine, or succinate were used as enzyme substrates, while using xanthine as a substrate increased significantly the xanthine oxidase production of ROS; this increase was prevented by incubation with the inhibitor allopurinol. Xan (Xanthine); Allop (Allopurinol). Data are reported as mean ± SD and analyzed with a two-tailed, unpaired Student's t test ($P < 0.05$). * indicate differences with respect to control.

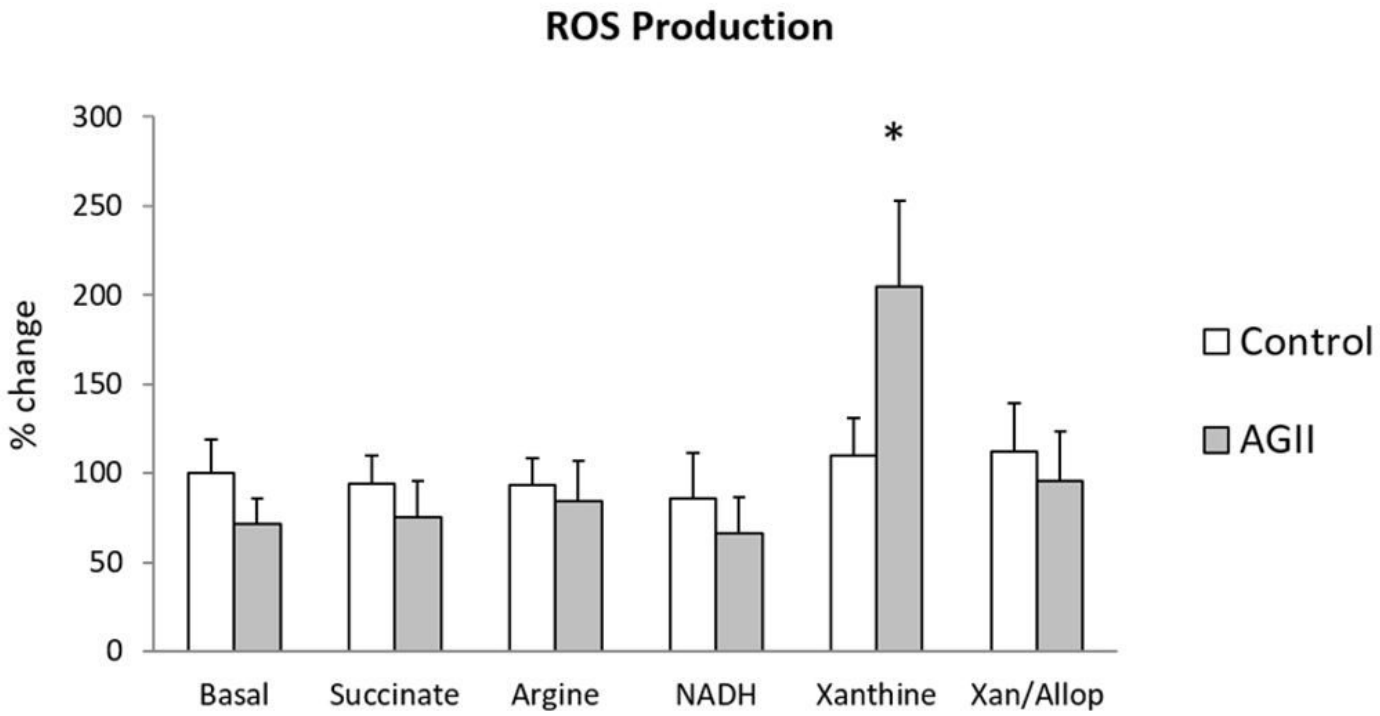

Figure 2

ROS production. AGII failed to induce changes in ROS production when NADH, arginine, or succinate were used as enzyme substrates, while using xanthine as a substrate increased significantly the xanthine oxidase production of ROS; this increase was prevented by incubation with the inhibitor allopurinol. Xan (Xanthine); Allop (Allopurinol). Data are reported as mean ± SD and analyzed with a two-tailed, unpaired Student's t test ($P < 0.05$). * indicate differences with respect to control.

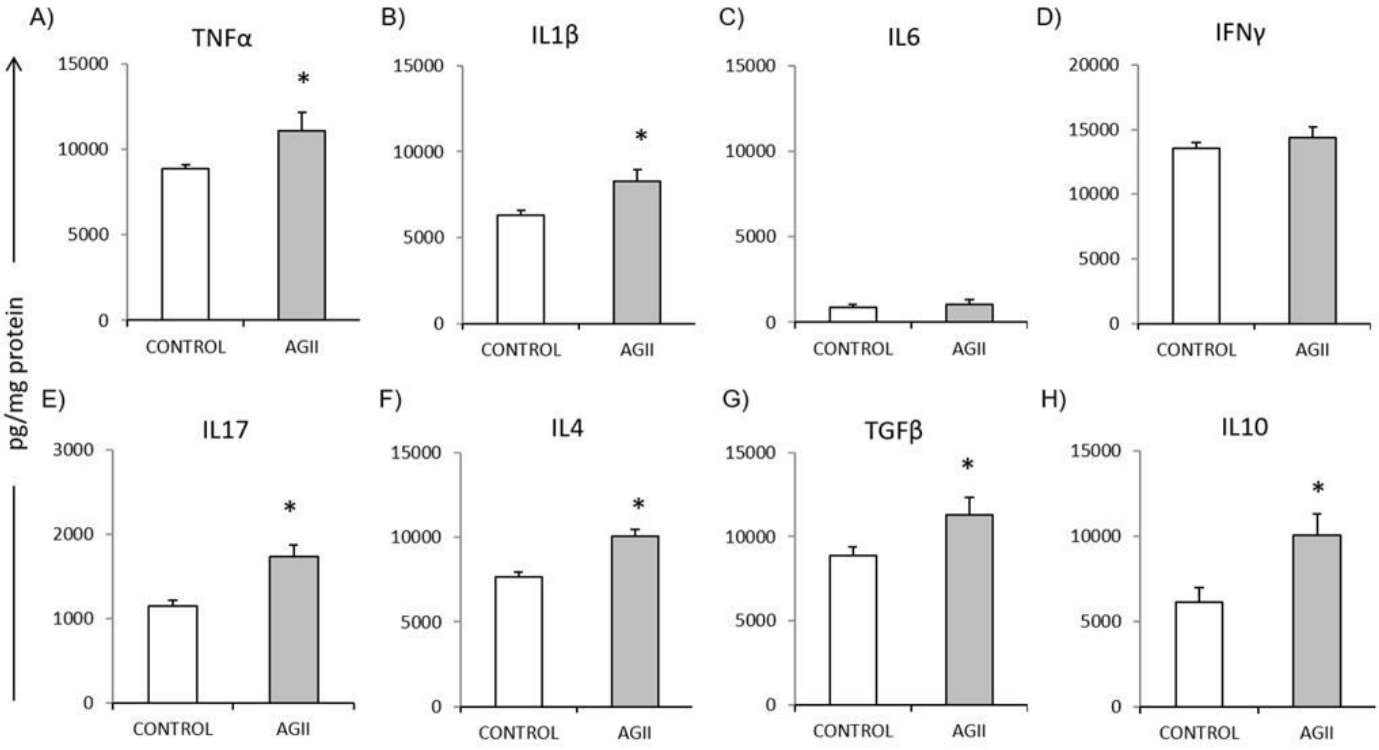

Figure 3

Cytokine concentrations in kidney. AGII administration for 10 weeks increased cytokine levels (A-H), both proinflammatory (A, B, E) and regulatory (G-H). Data are reported as mean ± SD and analyzed with a two-tailed, unpaired Student's t test ($P < 0.05$). * indicate differences with respect to control.

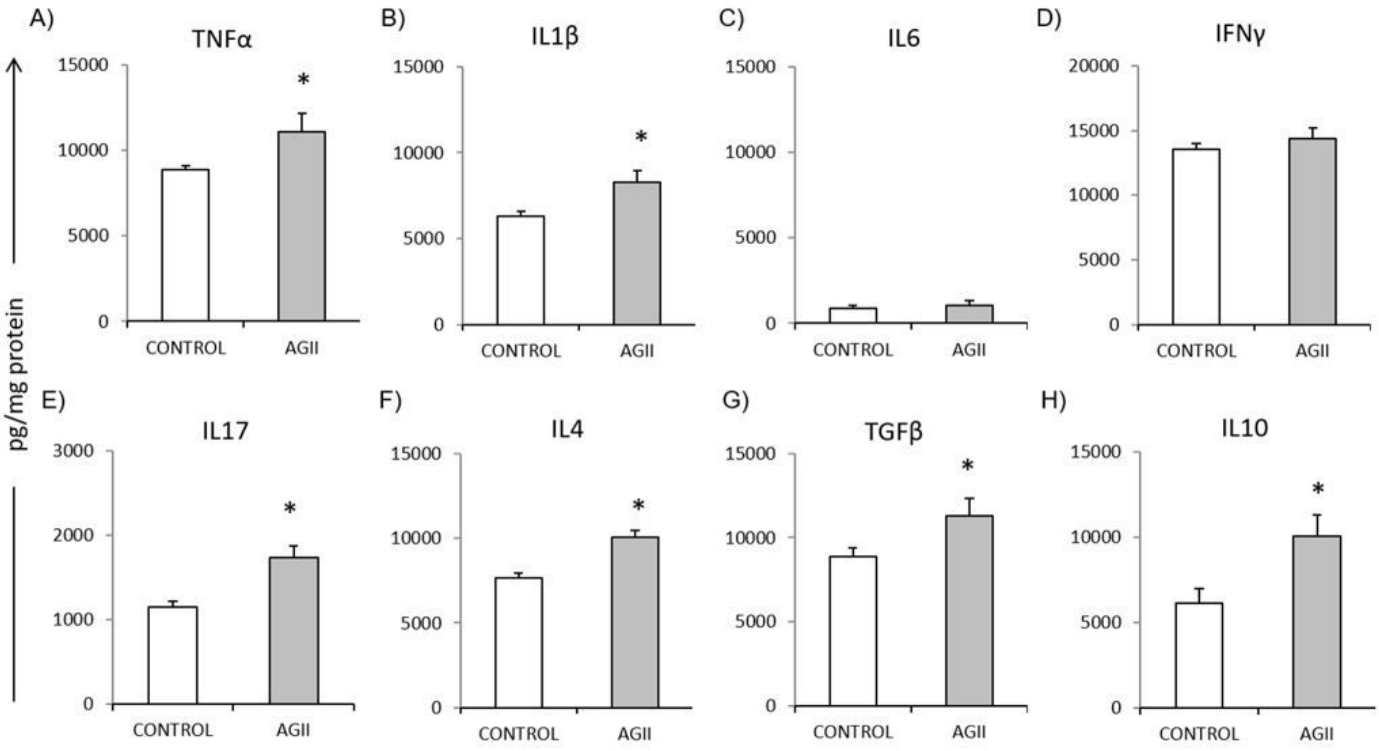

Figure 3

Cytokine concentrations in kidney. AGII administration for 10 weeks increased cytokine levels (A-H), both proinflammatory (A, B, E) and regulatory (G-H). Data are reported as mean ± SD and analyzed with a two-tailed, unpaired Student's t test ($P < 0.05$). * indicate differences with respect to control.

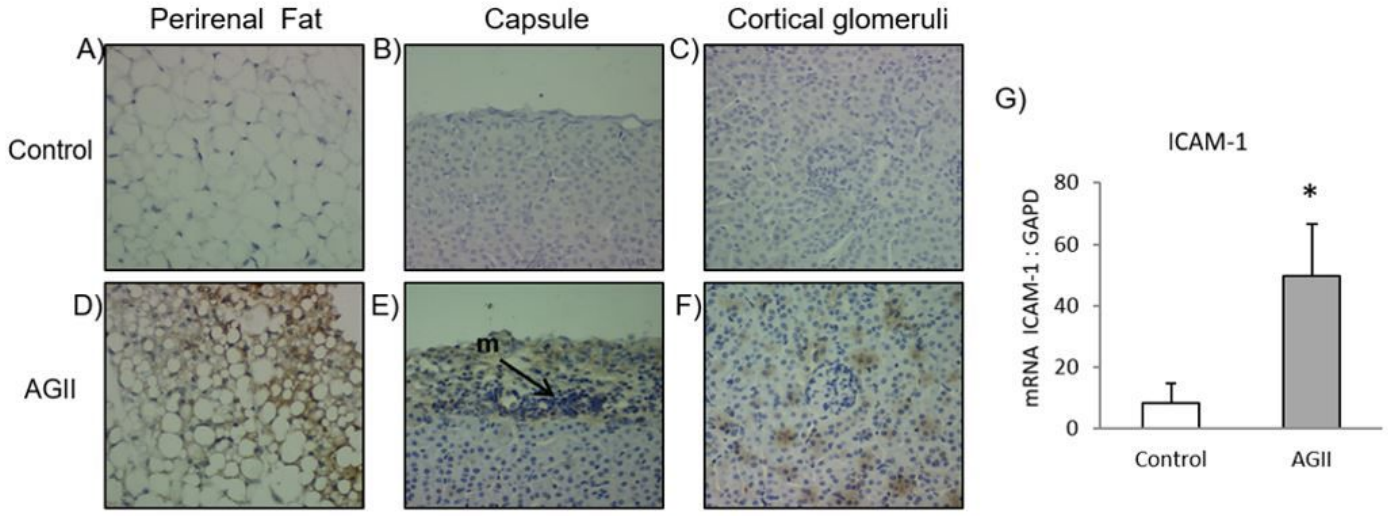

Figure 4

ICAM-1 expression detected by Immunohistochemistry. A-C) Control; D-F) AGII-administered group, G) Expression of ICAM-1 mRNA with respect to GADP mRNA. AGII induced an increase in ICAM-1 expression

in perirenal fat tissue (D), capsule (E), and renal interstice (F). Additionally, AGII increased the production of ICAM-1 mRNA; m: mononuclear cells. Microphotographs taken at 40X. Data are reported as mean ± SD and analyzed with a two-tailed, unpaired Student's t test (P < 0.05). * indicate differences with respect to control.

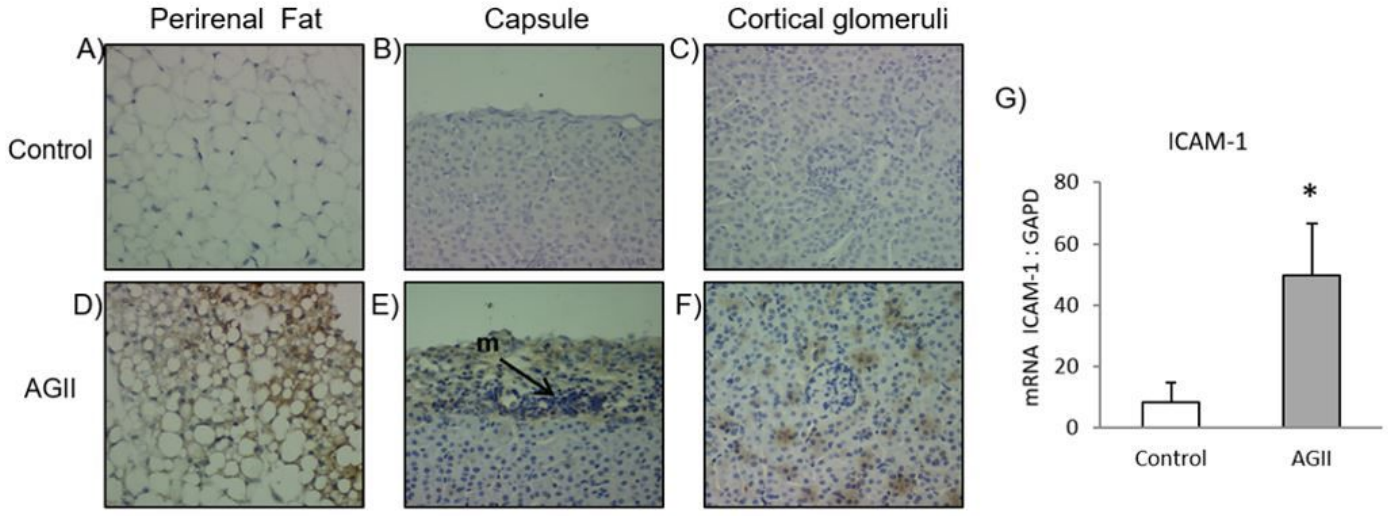

Figure 4

ICAM-1 expression detected by Immunohistochemistry. A-C) Control; D-F) AGII-administered group, G) Expression of ICAM-1 mRNA with respect to GADP mRNA. AGII induced an increase in ICAM-1 expression in perirenal fat tissue (D), capsule (E), and renal interstice (F). Additionally, AGII increased the production of ICAM-1 mRNA; m: mononuclear cells. Microphotographs taken at 40X. Data are reported as mean ± SD and analyzed with a two-tailed, unpaired Student's t test (P < 0.05). * indicate differences with respect to control.

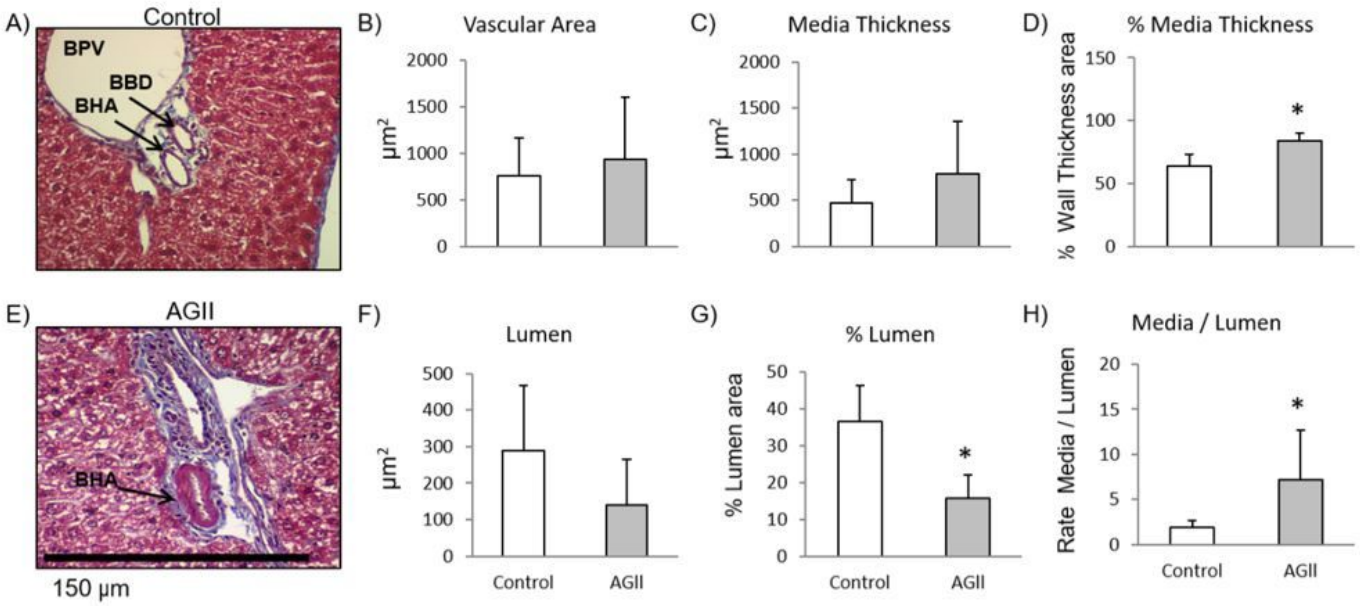

Figure 5

Evaluation of vascular remodeling in BHA by Masson trichrome staining. A-B) Hepatic portal triad from treated and control mice. C) Total BHA area. D) BHA lumen area. E) BHA medial thickness. F) Lumen and media (G) area percentage with respect to total BHA area. H) Media area/lumen area ratio. BHA thickening is a sign of vascular remodeling; BHA lumen measure was decreased in AGII-treated mice, while medial thickness and media/lumen ratio were increased. Microphotographs taken at 40X. (BPV) Branch of portal vein; (BHA) Branch of hepatic artery; (BBD) Branch of biliary duct. Data are reported as mean ± SD and analyzed with a two-tailed, unpaired Student's t test ($P < 0.05$). * indicate differences with respect to control.

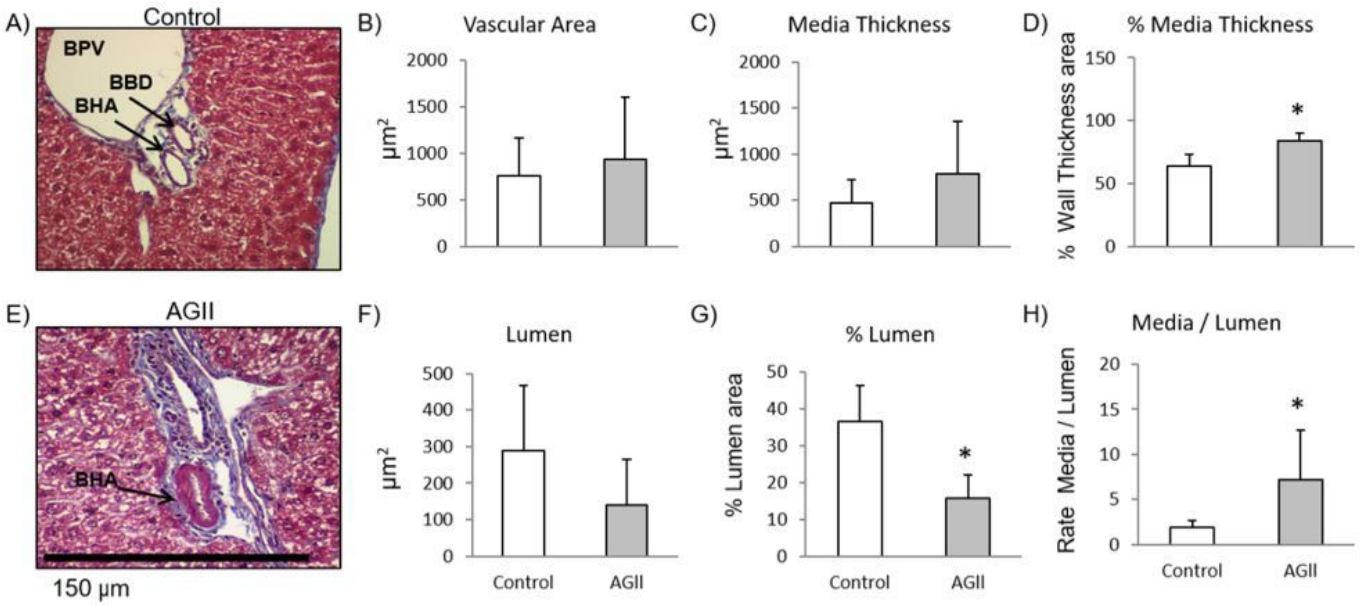

Figure 5

Evaluation of vascular remodeling in BHA by Masson trichrome staining. A-B) Hepatic portal triad from treated and control mice. C) Total BHA area. D) BHA lumen area. E) BHA medial thickness. F) Lumen and media (G) area percentage with respect to total BHA area. H) Media area/lumen area ratio. BHA thickening is a sign of vascular remodeling; BHA lumen measure was decreased in AGII-treated mice, while medial thickness and media/lumen ratio were increased. Microphotographs taken at 40X. (BPV) Branch of portal vein; (BHA) Branch of hepatic artery; (BBD) Branch of biliary duct. Data are reported as mean ± SD and analyzed with a two-tailed, unpaired Student's t test ($P < 0.05$). * indicate differences with respect to control.

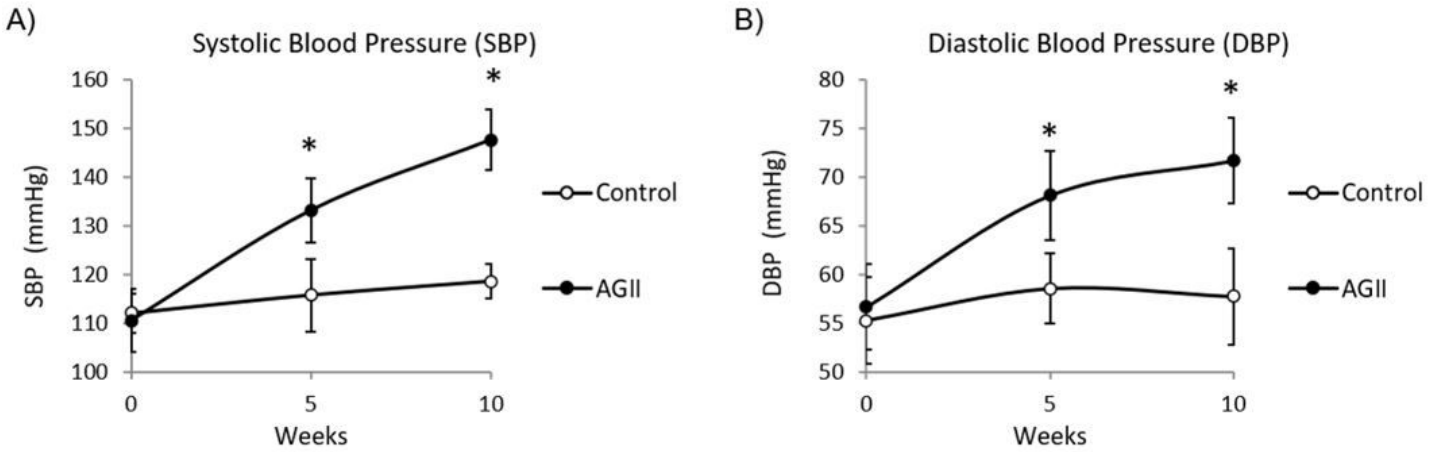

Figure 6

Time-course plot for blood pressure. A) Systolic blood pressure (SBP). B) Diastolic blood pressure (DBP). Blood pressure was measured in mice on weeks 0, 5, and 10. Both blood pressure values were increased in AGII-treated mice on weeks 5 and 10, and the animals were regarded as hypertensive. Data are reported as mean ± SD and analyzed with a two-tailed, unpaired Student's t test ($P < 0.05$). * indicate differences with respect to control.

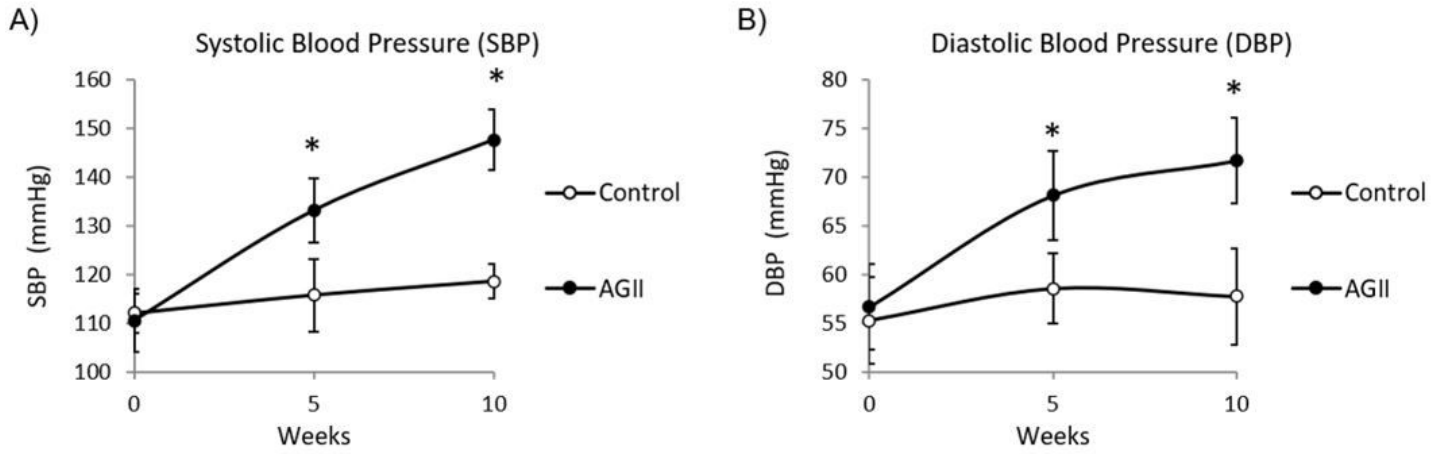

Figure 6

Time-course plot for blood pressure. A) Systolic blood pressure (SBP). B) Diastolic blood pressure (DBP). Blood pressure was measured in mice on weeks 0, 5, and 10. Both blood pressure values were increased in AGII-treated mice on weeks 5 and 10, and the animals were regarded as hypertensive. Data are reported as mean ± SD and analyzed with a two-tailed, unpaired Student's t test ($P < 0.05$). * indicate differences with respect to control.

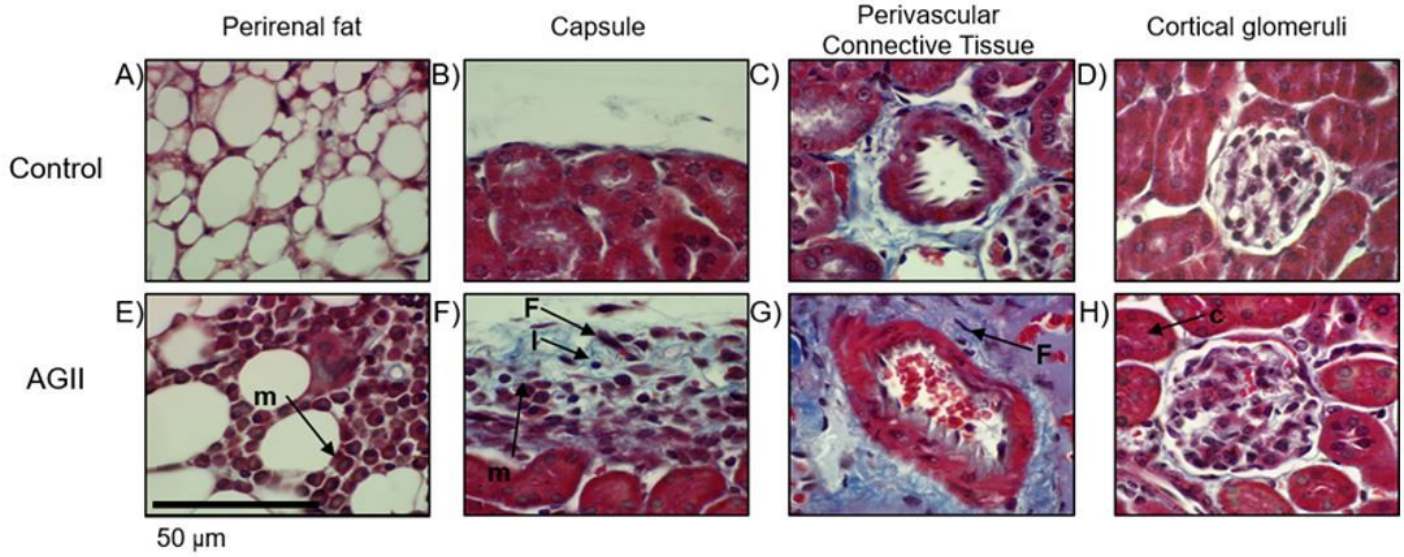

Figure 7

Evaluation of renal damage by Masson trichrome staining. A, E) Perirenal fat tissue. B, F) Renal capsule. C, G) Perivascular connective tissue. D, H) Cortical

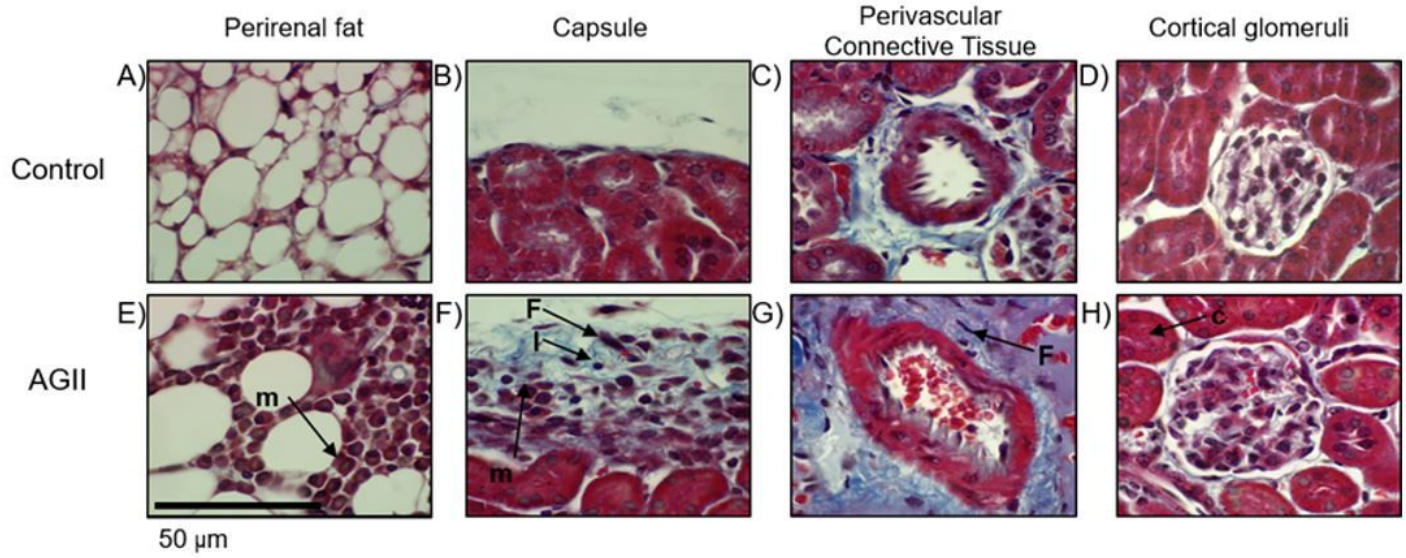

Figure 7

Evaluation of renal damage by Masson trichrome staining. A, E) Perirenal fat tissue. B, F) Renal capsule. C, G) Perivascular connective tissue. D, H) Cortical

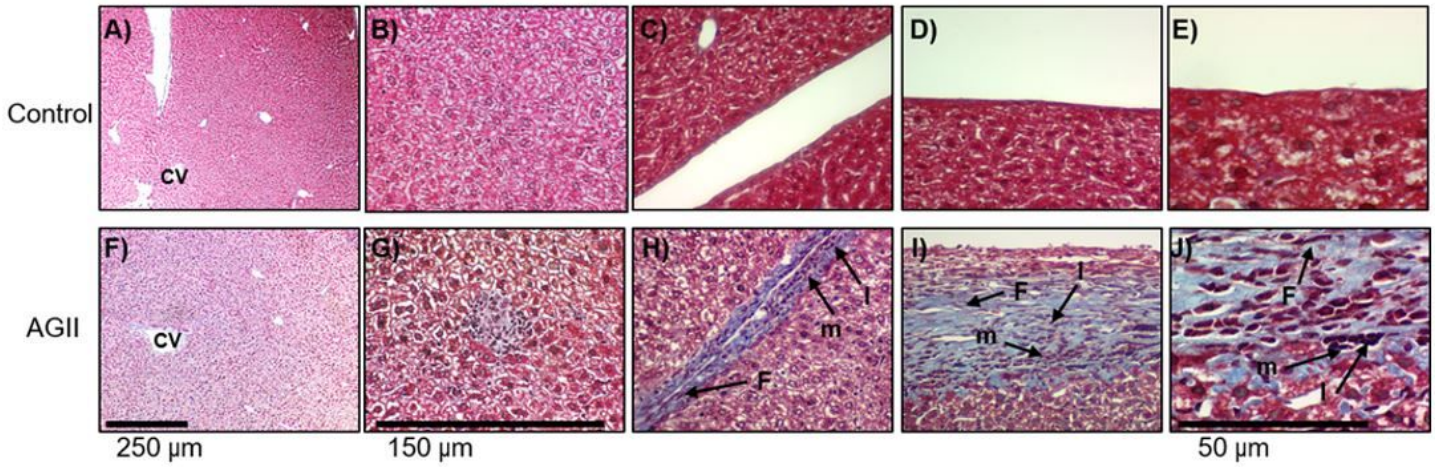

Figure 8

Evaluation of hepatic damage by Masson trichrome staining. A-B, F-G,) Hepatic parenchyma. C, H) Trabecuale. D-E, I-J) Glisson's capsule. AGII-treated mice showed steatohepatitis (F) and lymphocytic microabscesses (G). Additionally, trabeculae and Glisson's capsule showed mononuclear cell infiltrate and fiber deposition, leading to their thickening (H-J). CV: centrilobular veins; m: mononuclear inflammatory cells; F: fibroblasts; l: lymphocytes. Microphotographs taken at 10X (bar = 250 µm), 40X (bar = 150 µm) and 100X (bar = 50 µm).

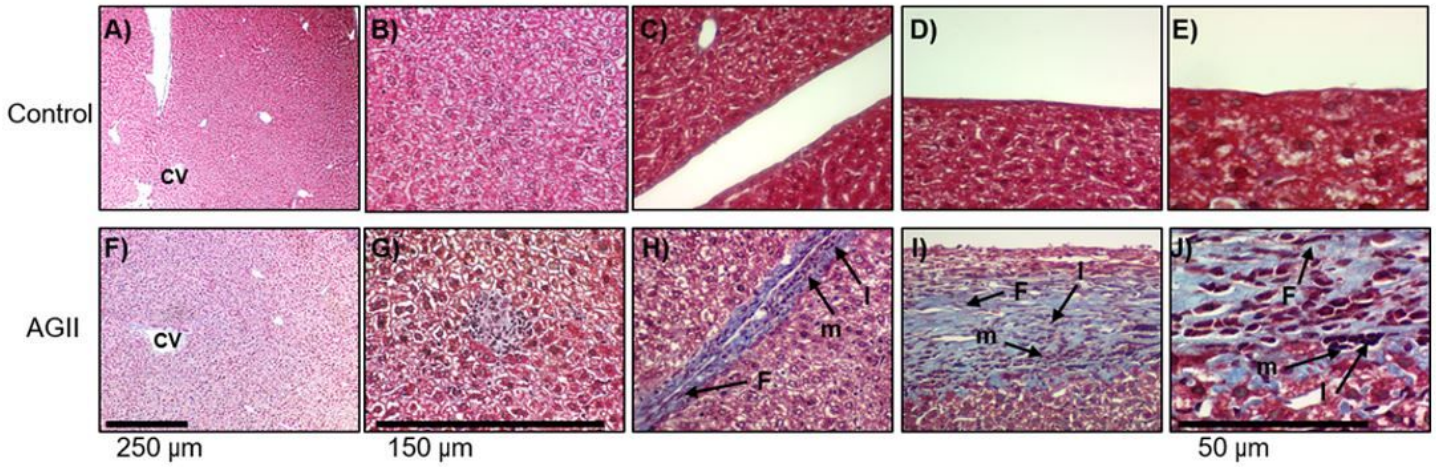

Figure 8

Evaluation of hepatic damage by Masson trichrome staining. A-B, F-G,) Hepatic parenchyma. C, H) Trabecuale. D-E, I-J) Glisson's capsule. AGII-treated mice showed steatohepatitis (F) and lymphocytic microabscesses (G). Additionally, trabeculae and Glisson's capsule showed mononuclear cell infiltrate and fiber deposition, leading to their thickening (H-J). CV: centrilobular veins; m: mononuclear inflammatory cells; F: fibroblasts; l: lymphocytes. Microphotographs taken at 10X (bar = 250 µm), 40X (bar = 150 µm) and 100X (bar = 50 µm).

Supplementary Files

This is a list of supplementary files associated with this preprint. Click to download.

- SupplementaryFigures.docx
- SupplementaryFigures.docx